Direct comparison of leaf plasmodesma structure and function in relation to phloem loading type

Liesche, Johannes; Gao, Chen; Binczycki, Piotr; Andersen, Signe Randi; Rademaker, Hanna; Schulz, Alexander; Martens, Helle Juel

Published in:
Plant Physiology

Link to article, DOI:
10.1104/pp.18.01353

Publication date:
2019

Document Version
Publisher's PDF, also known as Version of record

Direct Comparison of Leaf Plasmodesma Structure and Function in Relation to Phloem-Loading Type[1][OPEN]

Johannes Liesche,[a,b] Chen Gao,[a,b] Piotr Binczycki,[c] Signe R. Andersen,[c] Hanna Rademaker,[d] Alexander Schulz,[c,2] and Helle Juel Martens[c,3]

[a]College of Life Sciences, Northwest A&F University, Yangling 712100, China
[b]Biomass Energy Center for Arid and Semi-arid Lands, Northwest A&F University, Yangling 712100, China
[c]Department of Plant and Environmental Sciences, University of Copenhagen, DK-1871 Frederiksberg, Denmark
[d]Department of Physics, Technical University of Denmark, 2800 Kongens Lyngby, Denmark

ORCID IDs: 0000-0001-8753-4037 (J.L.); 0000-0001-6796-3598 (A.S.); 0000-0002-3011-4557 (H.J.M.).

The export of photosynthetically produced sugars from leaves depends on plasmodesmatal transport of sugar molecules from mesophyll to phloem. Traditionally, the density of plasmodesmata (PD) along this phloem-loading pathway has been used as a defining feature of different phloem-loading types, with species proposed to have either many or few PD between the phloem and surrounding cells of the leaf. However, quantitative determination of PD density has rarely been performed. Moreover, the structure of PD has not been considered, even though it could impact permeability, and functional data are only available for very few species. Here, a comparison of PD density, structure, and function using data from transmission electron microscopy and live-cell microscopy was conducted for all relevant cell–cell interfaces in leaves of nine species. These species represent the three principal phloem-loading types currently discussed in literature. Results show that relative PD density among the different cell-cell interfaces in one species, but not absolute PD density, is indicative of phloem-loading type. PD density data of single interfaces, even combined with PD diameter and length data, did not correlate with the intercellular diffusion capacity measured by the fluorescence loss in photobleaching method. This means that PD substructure not visible on standard transmission electron micrographs may have a strong influence on permeability. Furthermore, the results support a proposed passive symplasmic loading mechanism in the tree species horse chestnut (*Aesculus hippocastanum*), white birch (*Betula pubescens*), orchard apple (*Malus domestica*), and gray poplar (*Populus x canescens*) as functional cell coupling and PD structure differed from active symplasmic and apoplasmic phloem-loading species.

A key step in the export of photosynthetically produced sugars from the leaf is the loading into the phloem sieve elements (SEs). Once inside the SEs, the sugars are moved by mass flow of phloem sap toward sink tissues. Three principal types of phloem loading have been defined depending on the energy requirement (active or passive) and plasmodesmata (PD)-mediated cell coupling between cells leading up to the SEs, i.e. the capacity of sugars to diffuse from mesophyll to phloem SEs (apoplasmic or symplasmic; Liesche and Patrick, 2017; Zhang and Turgeon, 2018). In many herbaceous plants, including most crop plants, sugar transporters are responsible for the active uptake of sugars into the complex of companion cell and SE companion cell complex (SECCC). In these plants, the SECCC is assumed to be symplasmically isolated (Braun, 2012), leading to the designation of "active apoplasmic" loading type. In many tree species it has been proposed that numerous PD enable sugar diffusion into the SEs, whereas active processes are not directly involved in phloem loading (Fu et al., 2011; Schulz, 2015). This loading type is referred to as "passive symplasmic" loading. In "active symplasmic" loading, found in herbaceous as well as woody plant species, low M_r sugars can diffuse into the SECCC, where they are actively oligomerized. This prevents their diffusion back into the surrounding leaf cells.

Although the PD-mediated, functional cell coupling is a defining feature of the mechanism of phloem loading, it has been quantified in only a handful of species. The phloem-loading pathway commences in the mesophyll cells (MCs), where most of the sugars are produced, via the bundle sheath cells (BSCs), and in some cases the vascular parenchyma cells (VPCs) to the

[1]This work was supported by the National Natural Science Foundation of China (NSFC grant 31872699 to J.L.).
[2]Author for contact: als@plen.ku.dk.
[3]Senior author.
The author responsible for distribution of materials integral to the findings presented in this article in accordance with the policy described in the Instructions for Authors (www.plantphysiol.org) is: Alexander Schulz (als@plen.ku.dk).

J.L., A.S., and H.J.M. conceived the project and research plan; J.L., C.G., P.B., S.R.A., and H.R. carried out the experiments; J.L., C.G., and H.J.M. analyzed the data; J.L. and H.J.M. wrote the article with contributions of all the authors; A.S. agrees to serve as the author responsible for contact and ensure communication.

[OPEN]Articles can be viewed without a subscription.
www.plantphysiol.org/cgi/doi/10.1104/pp.18.01353

SECCC. Quantification of functional cell coupling between the different cells along the phloem-loading pathway demonstrated that indeed coupling between BSCs and SECCC is low in the active apoplasmic loaders tobacco (*Nicotiana tabacum*) and fava bean (*Vicia faba*), while it is high in the active apoplasmic loader *Cucurbita maxima* and the putative passive symplasmic loader *Pinus sylvestris* (Liesche and Schulz, 2012). In all other cases, functional cell coupling was deduced from the PD density, or absence of PD, as seen on electron micrographs (Gamalei, 1989, 1991; Fu et al., 2011; Batashev et al., 2013;). However, PD density does not necessarily correspond to permeability (Oparka and Prior, 1992; Schulz, 1995). A direct comparison of PD density and function has never been attempted. This would be especially relevant for the many angiosperm trees that were designated as "passive symplasmic" loaders (Davidson et al., 2011; Fu et al., 2011). Although for plants of the active loading types there is broad agreement on the validity of their phloem-loading mechanism, the feasibility of passive symplasmic loading is still under debate (Öner-Sieben and Lohaus, 2014; Liesche, 2017; Fink et al., 2018). For some trees, a high PD density between BSCs and SECCC has been reported, which is in line with passive symplasmic loading, even though evidence for the involvement of sugar transporters in the loading process was found (Goggin et al., 2001; Turgeon and Medville, 2004; Öner-Sieben and Lohaus, 2014; Fink et al., 2018). Calculations showed that active transporter-mediated phloem loading would be compromised by open PD as they would result in back-flow of the transported sugars (Liesche, 2017). The lack of quantitative data on functional cell coupling in angiosperm trees prevents any conclusion in the direction of nonfunctional PD potentially facilitating active transporter-mediated loading.

In this study, we collected anatomical data on PD in the prephloem pathway as well as functional data on cell coupling to show if PD density measured from electron micrographs correlates with functional cell coupling, tested by live-cell microscopy of fluorescent tracer diffusion. For the electron microscopic quantification of PD density, standards developed by Robards (1976) and Botha and van Bel (1992) were followed. PD density per μm vein, along the vein axis, was determined, because this parameter is more relevant than PD density per μm^2 cell wall for the comparative analysis of the transport capacity along the phloem-loading pathway across species (Botha and van Bel, 1992). Furthermore, it was investigated to what extent different PD structures, as determined from electron microscopy, influence permeability. Permeability was assessed by quantifying intercellular movement of a fluorescent tracer with similar diffusion properties to Suc (Liesche and Schulz, 2013) in fluorescence loss in photobleaching (FLIP) experiments. The study includes nine species assigned to the three different loading types (Table 1), which should allow for an assessment of the degree of variability between species of the same loading type and generalization of results. Tobacco represents the active apoplasmic phloem-loading type with true companion cells (CCs; Liesche and Schulz, 2012). Fava bean and primrose (*Primula vulgaris*) represent active apoplasmic loading with CCs modified as transfer cells (Gamalei, 1989). Pumpkin (*Cucurbita pepo*) and verbena (*Verbena bonariensis*) represent active symplasmic loading (Gamalei, 1989). Horse chestnut (*Aesculus hippocastanum*), white birch (*Betula pubescens*), orchard apple (*Malus domestica*), and gray poplar (*Populus x canescens*) represent the predicted passive symplasmic loading type (Gamalei, 1989; Fu et al., 2011).

RESULTS

Minor Vein Anatomy

The anatomy of the minor veins showed a high level of similarity, which is a prerequisite for making comparative analyses. The minor veins of all species examined contained a bundle sheath consisting of 6–10 large cells and 3–5 SEs (Fig. 1), and in addition to SEs and CCs, VPCs and xylem vessels were present in all minor veins. In most species, no differentiation between xylem parenchyma and phloem parenchyma could be

Table 1. *Information on specimens used in this study*

The classification of presumed phloem-loading type is based on Rennie and Turgeon (2009) and Fu et al. (2011). *n* = number of minor veins analyzed by TEM and FLIP experiments; all plants were grown in the Copenhagen area; gray poplar is a hybrid between white poplar (*Populus alba*) and common aspen (*Populus tremula*).

Species	Common Name	Acronym	Family	Plant Size, Habit, and Growth Environment	Presumed Phloem-Loading Type	*N* (TEM)	*N* (FLIP)
Aesculus hippocastanum	Horse chestnut	AES	Sapindacea	10 m tree height, parking area	Passive symplasmic	16	3
Betula pubescens	White birch	BET	Betulaceae	2 m tree height, garden	Passive symplasmic	43	12
Malus domestica	Orchard apple	MAL	Rosaceae	3 m tree height, garden	Passive symplasmic	45	10
Populus x canescens	Gray poplar	POP	Salicaceae	10 m tree height, park	Passive symplasmic	10	10
Nicotiana tabacum	Tobacco	NIC	Solanaceae	Annual herbaceous, greenhouse	Active apoplasmic	6	13
Primula vulgaris	Primrose	PRI	Primulaceae	Perennial herbaceous, garden	Active apoplasmic	4	5
Vicia faba	Fava bean	VIC	Fabaceae	Annual herbaceous, greenhouse	Active apoplasmic	6	10
Cucurbita pepo	Pumpkin	CUC	Cucurbitaceae	Annual herbaceous, greenhouse	Active symplasmic	5	15
Verbena bonariensis	Verbena	VER	Verbenaceae	Perennial herbaceous, garden	Active symplasmic	8	—

made based on appearance. The cross-sectional diameter of the minor veins of all tested plants is very similar, with values between 35 and 50 μm (Fig. 1). In addition, the length of the interfaces between MCs and BSCs, and the combined area of the SEs in one minor vein, were found to be similar across species (Fig. 1). SEs are always in contact with CCs. In all species, BSCs are in contact with VPCs, which, in turn, are in contact with CCs and SEs. CCs appear directly next to BSCs in the images shown in Figure 1, while in other sections this contact might not be visible.

CC characteristics can be indicative of the phloem-loading type. CCs with abundant wall ingrowths have been termed "transfer cells," as their strongly increased cell surface was proposed to correlate with increased sugar transfer across their plasma membrane, which has been confirmed for Arabidopsis (*Arabidopsis thaliana*) and pea (*Pisum sativum*; Adams III et al., 2014). Transfer cell-like CCs are apparent here in the herbaceous species *f*ava bean and primrose, but surprisingly, also in the proposed passive symplasmic loader horse chestnut (Fig. 2). The CCs of pumpkin (Fig. 1F) and verbena show the abundant, asymmetrically branched PD, which are only found in active symplasmic loaders and are usually referred to as intermediary cells (Fig. 3J).

Plasmodesmatal Density

The density of PD was determined for each interface along the phloem-loading pathway using transmission electron microscopy (TEM). PD counts were specified per unit length of minor vein, instead of per μm^2 interface, to reflect the total capacity for sugar diffusion toward SEs (Botha and van Bel, 1992). The total number of PD along the whole phloem-loading pathway corresponding to a 1-μm–long segment of the minor vein

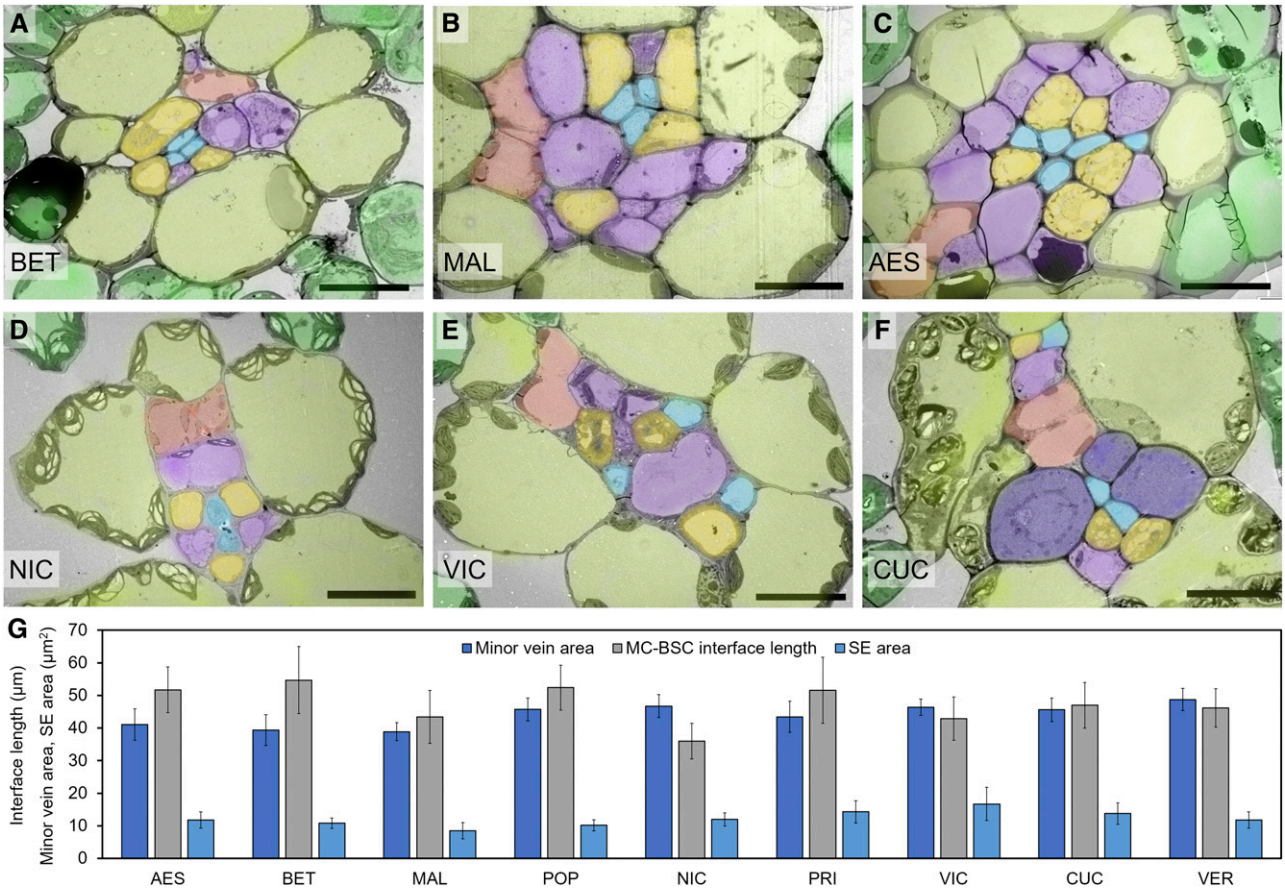

Figure 1. Anatomy of minor veins in species with different phloem-loading types. A–D, Overview images of minor veins with colors indicating the different cell types: MCs (dark green), BSCs (light green), xylem (orange), vascular parenchyma (light purple), CCs (yellow), SEs (light blue), and intermediary-type CCs (dark purple). The general anatomy is similar between the presumed passive symplasmic loaders *Betula pubescens* (BET; A), *Malus domestica* (MAL; B), and *Aesculus hippocastanum* (AES; C) and the active apoplasmic loaders *Nicotiana tabacum* (NIC; D) and *Vicia faba* (VIC; E) and the active symplasmic loader *Cucurbita pepo* (CUC; F); for species' Latin, common names, and acronyms, see Table 1. Quantification confirms that minor vein cross-sectional area, mesophyll-bundle sheath interface length, and total SE area are similar between all tested plants (G). $n \geq 4$. Error bars = SD. Scale bars = 10 μm. POP, *Populus x canescens*; PRI, *Primula Vulgaris*; VER, *Verbena bonariensis*.

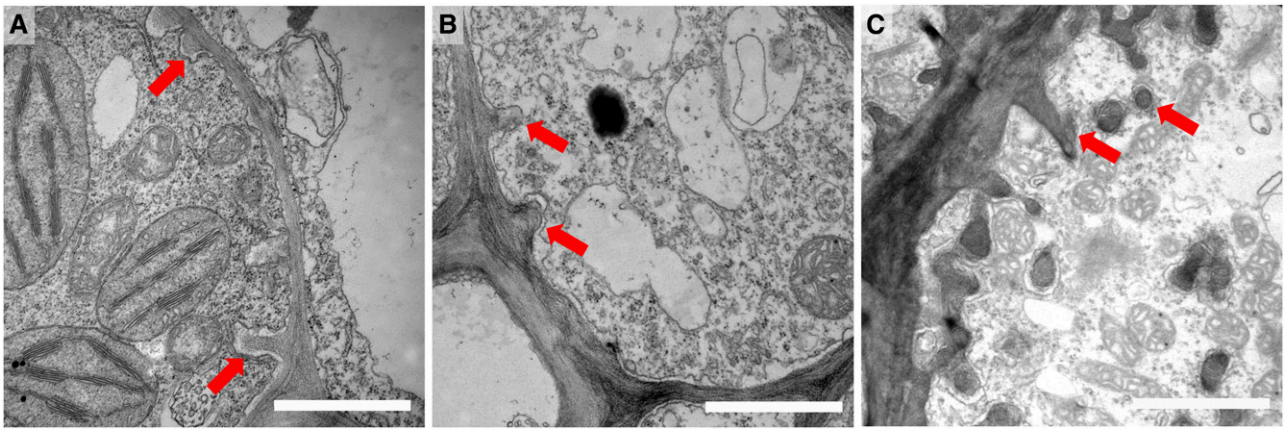

Figure 2. Wall ingrowths in CCs. A and B, Wall ingrowths (arrows) have been previously observed in active apoplasmic phloem loaders such as *Vicia faba* (A) and *Primula vulgaris* (B). The tree *Aesculus hippocastanum*, a presumed passive symplasmic loader, was found to have highly elaborate wall ingrowths in CCs (C). Scale bars = 1 μm.

varied between 155 in orchard apple and 1,717 in pumpkin (Fig. 4). The sum of PD was several times higher in the active symplasmic loaders pumpkin and verbena than in the seven species of other loading types, for which numbers ranging between 155 and 387 were recorded (Fig. 4).

The comparison of PD density at the different interfaces across species revealed large differences, even between species that are assumed to have the same phloem-loading types (Fig. 5). The number of PD at the different interfaces in orchard apple were at least two times lower than at the corresponding interface in horse chestnut (Fig. 5A). Similarly, PD density in primrose was between 1.5 and 3 times lower compared to tobacco (Fig. 5A). Indeed, PD density at the VPC:CC interface that is critical for apoplasmic phloem loading is similar for the apoplasmic loader tobacco and the presumed passive symplasmic loader orchard apple (Fig. 5A). However, a principal difference between the presumed passive loaders and active apoplasmic loaders becomes apparent when comparing relative PD density (Fig. 5B). Although PD were present between VPCs and CCs and between VPCs and BSCs in all apoplasmic loaders, their density was lower compared to the interfaces upstream along the phloem-loading pathway (Fig. 5B). A similar difference in PD density was not observed in the presumed passive symplasmic loaders, where, instead, PD are distributed at relatively similar numbers along the whole pathway (Fig. 5B). The active symplasmic loaders pumpkin and verbena show a distinctly different pattern from all species with other loading type. PD density at their BSC-CC interface was many times higher as compared to the upstream interfaces (Fig. 5).

Functional Cell Coupling

To measure the PD-mediated interface permeability in vivo, we conducted FLIP experiments (Fig. 6). Control experiments were performed on mature guard cells, which are known to be symplasmically isolated from surrounding epidermis cells (Martens et al., 2006). These show a 10% signal decrease in guard cells after bleaching the neighboring epidermal cell (Supplemental Fig. S1). This decrease is considered the baseline and might result from tracer movement across membranes instead of through PD and/or bleaching by excitation light scattering and reflection at cell structures. For the test of functional cell coupling along the phloem-loading pathway, BSCs were chosen as target cells for the bleaching as it afforded concomitant observation of the diffusion-driven signal reduction in the neighboring MCs and SECCC. No differentiation could be made between CCs and SEs.

Regarding functional cell coupling between MCs and BSCs, similar values of ~30% signal decrease were recorded for all species, with only horse chestnut showing a significantly higher signal decrease (Fig. 6E). Coupling across the BSC:SECCC interface showed higher variability. The four tree species had a relatively high signal decrease of ~40% (Fig. 6E). The decrease was even higher in the active symplasmic loader pumpkin (Fig. 6E). In the active apoplasmic loaders tobacco, primrose, and fava bean, the signal decrease was significantly lower than in the other species, but still ~20% higher than the baseline determined in the control experiment (Fig. 6E; Supplemental Fig. S1).

Structure–Function Relationship of PD Along the Phloem-Loading Pathway

For a detailed evaluation of the relationship between the results obtained by TEM and those obtained by FLIP, the structure of PD as seen on TEM images was analyzed. The TEM images enabled the measurement of PD diameter and length. While PD length scales negatively with permeability, the relationship of PD diameter to permeability is not clear as this depends on

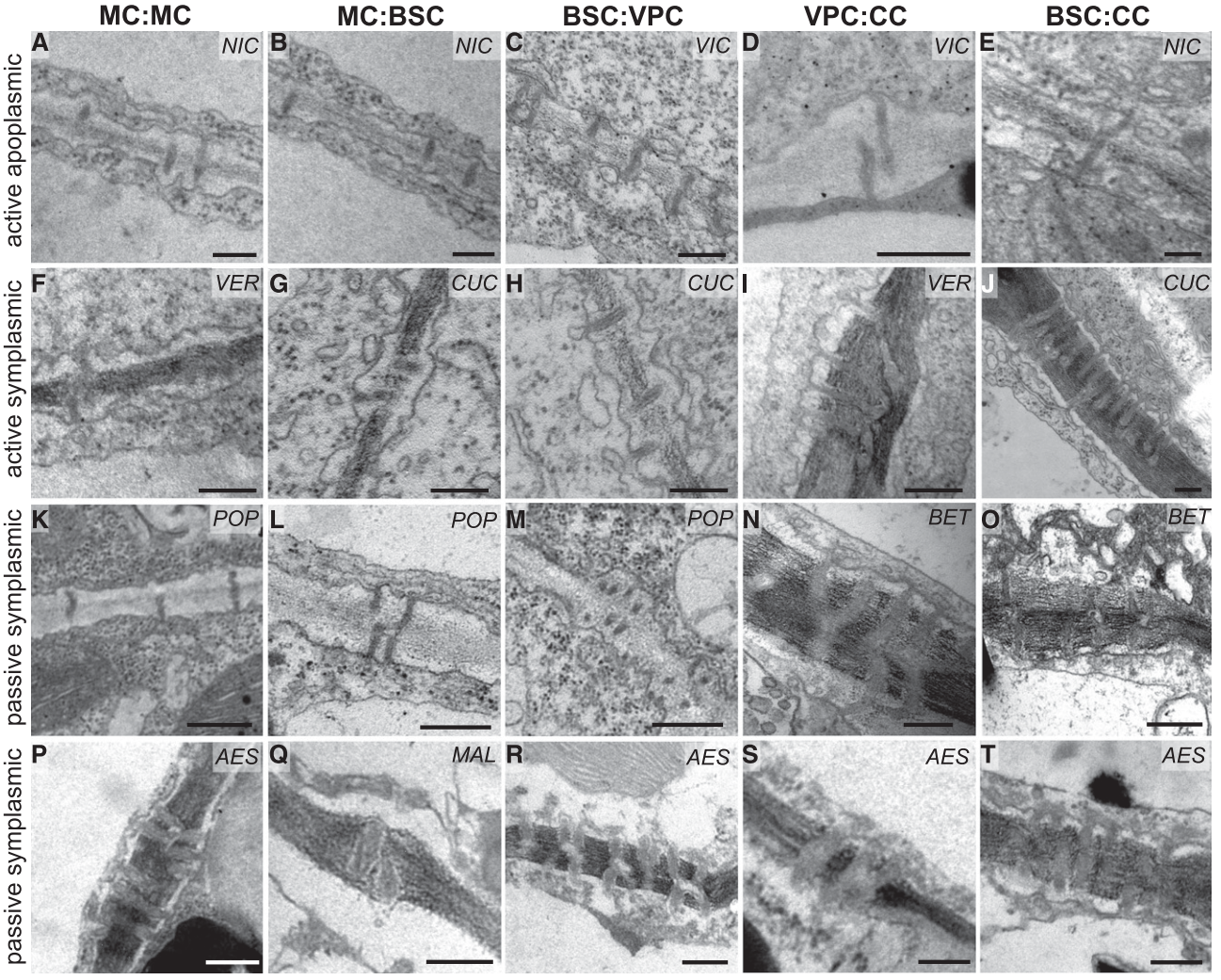

Figure 3. PD at cellular interfaces along the phloem-loading pathway. Transmission electron micrographs of PD at different interfaces. Representative images are shown for apoplasmic loaders (ACT.APO.) *Nicotiana tabacum* (*NIC*) and *Vicia faba* (*VIC*; A–E), active symplasmic loaders (ACT.SYM.) *Verbena bonariensis* (VER) and *Cucurbita pepo* (CUC; F–J) and for the putative passive symplasmic loaders (PAS.SYM.) *Betula pubescens* (*BET*), *Populus x canescens* (*POP*), *Malus domestica* (*MAL*), and *Aesculus hippocastanum* (*AES*; K–T). Scale bars = 200 nm.

PD substructure, which has not been determined at sufficient resolution so far (Liesche and Schulz, 2013). We therefore used the diameter raw values as well as a hindrance factor that is based on the PD diameter minus the desmotubule diameter. This means that presence of an unobstructed cytoplasmic sleeve inside each PD was assumed. As the width of the cytoplasmic sleeve could not be determined from TEM images, a desmotubule diameter of 19 nm was assumed, which is 1-μm smaller than the smallest PD diameter measured here and at the higher end of previous estimates (Schulz, 1995; Knox et al., 2015; Nicolas et al., 2017).

The analysis of PD diameter and length showed that in passive symplasmic loaders, PD were generally wider at the MC:MC and MC:BSC interfaces, but similar at the downstream interfaces (Fig. 7). Active apoplasmic loaders have relatively narrow PD at the BSC:VPC interface. However, they are of similar width and length compared to the four tree species (Fig. 7, A and C). The situation is similar for the VPC:CC interface. Interestingly, the PD at the BSC:CC interface in active symplasmic loaders, whose structure is supposed to be essential for their function in phloem loading (Liesche and Schulz, 2013), are not smaller in diameter than those at some other interfaces in the same and other species (Fig. 7, A–C). While these PD are longer than in the other interfaces of the active symplasmic loaders (Fig. 7C), PD of similar length were observed in other species, for example gray poplar and orchard apple at the VPC:CC interface (Fig. 7A).

A correlation analysis of structural parameters and the functional data from the FLIP experiments was performed (Fig. 7D). *P* values that describe the likelihood of correlation were compared for the single factors: density, diameter, length, hindrance; and combined

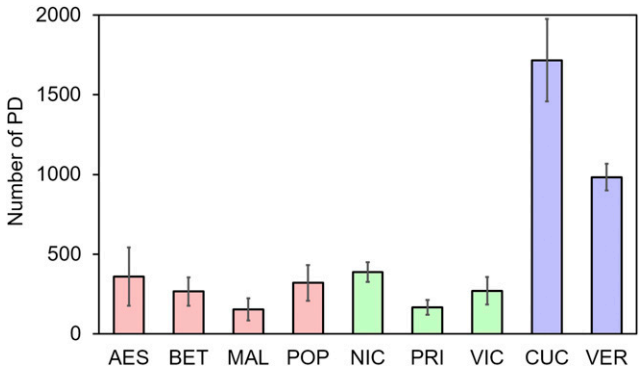

Figure 4. Total number of PD at all interfaces along the phloem-loading pathway of a vein segment of 1-μm length. Colors refer to the presumed phloem-loading types: passive symplasmic loading (red), active apoplasmic loading (green), and active symplasmic loading (purple). Error bars = SD. AES, *Aesculus hippocastanum*; BET, *Betula pubescens*; MAL, *Malus domestica*; POP, *Populus x canescens*; NIC, *Nicotiana tabacum*; PRI, *Primula vulgaris*; VIC, *Vicia faba*; CUC, *Cucurbita pepo*; VER, *Verbena bonariensis*.

parameters: radius divided by length, hindrance divided by length, hindrance times density, density divided by length, diameter times density, hindrance times density, as well as diameter divided by length times density and hindrance divided by length times density. For the data of the MC:BSC interface, the lowest *P* value was calculated for the correlation of FLIP results with the product of PD diameter times density (Fig. 7D). However, with a value >0.05, the correlation cannot be considered significant. For the data of the BSC:SECCC interface, significant correlation of structural and functional values was found for relative PD density, diameter times density, and hindrance times density (Fig. 7D). The structural factors used here were the average values of the BSC:VPC and the VPC:CC interfaces. These average values showed lower *P* values than either data from the BSC:VPC or VPC:CC or BSC:CC interface considered alone (data not shown). The exception is pumpkin, for which only the BSC:CC interface was considered.

Considering both interfaces, diameter times density appears as the most reliable parameter to estimate PD-mediated interface permeability. PD length appears not relevant. Hindrance, which is based on diameter, does not improve correlation (Fig. 7D), indicating that the cytosolic sleeve model (Liesche and Schulz, 2013) is not an accurate representation of PD substructure. Furthermore, it should be noted that while relative density provides good correlation for the BSC:phloem interface, it has the highest *P* value of all parameters for the BSC:MC interface (Fig. 7D).

Correlation coefficients for correlations between relative density and diameter times density for the BSC:SECCC interface are high (Fig. 7D), reflecting the pronounced differences in density, even though functional differences are moderate.

DISCUSSION

Relative Density Indicates Phloem-Loading Type

Among the nine species tested here, the relative distribution of PD along the different interfaces of the phloem-loading pathway proved indicative of the phloem-loading type. A similar observation was made by Botha and van Bel (1992) who assembled data for several active apoplasmic and active symplasmic loading species. The tests on functional cell coupling conducted here show that the relative density does indeed correspond to the capacity for intercellular diffusion of small molecules between the SECCC and surrounding cells, which is decisive for the phloem-loading mechanism.

The results are remarkable as they show that only relative, but not absolute PD density correlates with PD-mediated interface permeability. For example, orchard apple showed similar coupling across the BSC:phloem interface as white birch and gray poplar even though the latter species have approximately twice the number of PD at the relevant interfaces. This discrepancy cannot be explained by the slightly wider PD. Indeed, species-specific differences in the PD substructure that are not visible on TEM images must influence permeability so that the phloem-loading capacity becomes independent of absolute PD numbers when comparing species of the same loading type. While, in principle, nonhomogeneous distribution of PD could lead to inaccurate PD counts, the high number of analyzed minor vein sections, >40 for orchard apple and white birch, make this unlikely.

TEM Images Cannot Predict Permeability of a Specific Interface

It has previously been suggested that the functionality of PD cannot be inferred from their appearance on TEM images, because PD could be regulated dynamically (Schulz, 1999; Roberts and Oparka, 2003; Liesche and Schulz, 2012). Results presented here prove that absolute PD density is an inadequate measure of PD-mediated cell wall permeability. Neither for the MC:BSC- nor the BSC:SECCC-interface did absolute density correlate with permeability as measured by FLIP experiments. For the BSC:SECCC interface, taking the PD diameter into account, in addition to density, achieved correlation with permeability. However, for the BSC:MC interface, no significant correlation could be found for any structural parameter or their combinations. This shows that even quantitative TEM data are insufficient. It should be noted that only the standard TEM procedure was employed here. TEM tomography, computer-aided reconstruction (e.g. Ding et al., 1992; Nicolas et al., 2017) and other methods that provide additional resolution could potentially improve the predictive capacity of EM images. However, functional tests, like the relatively simple live-cell microscopy method with fluorescent tracer, will always be preferable.

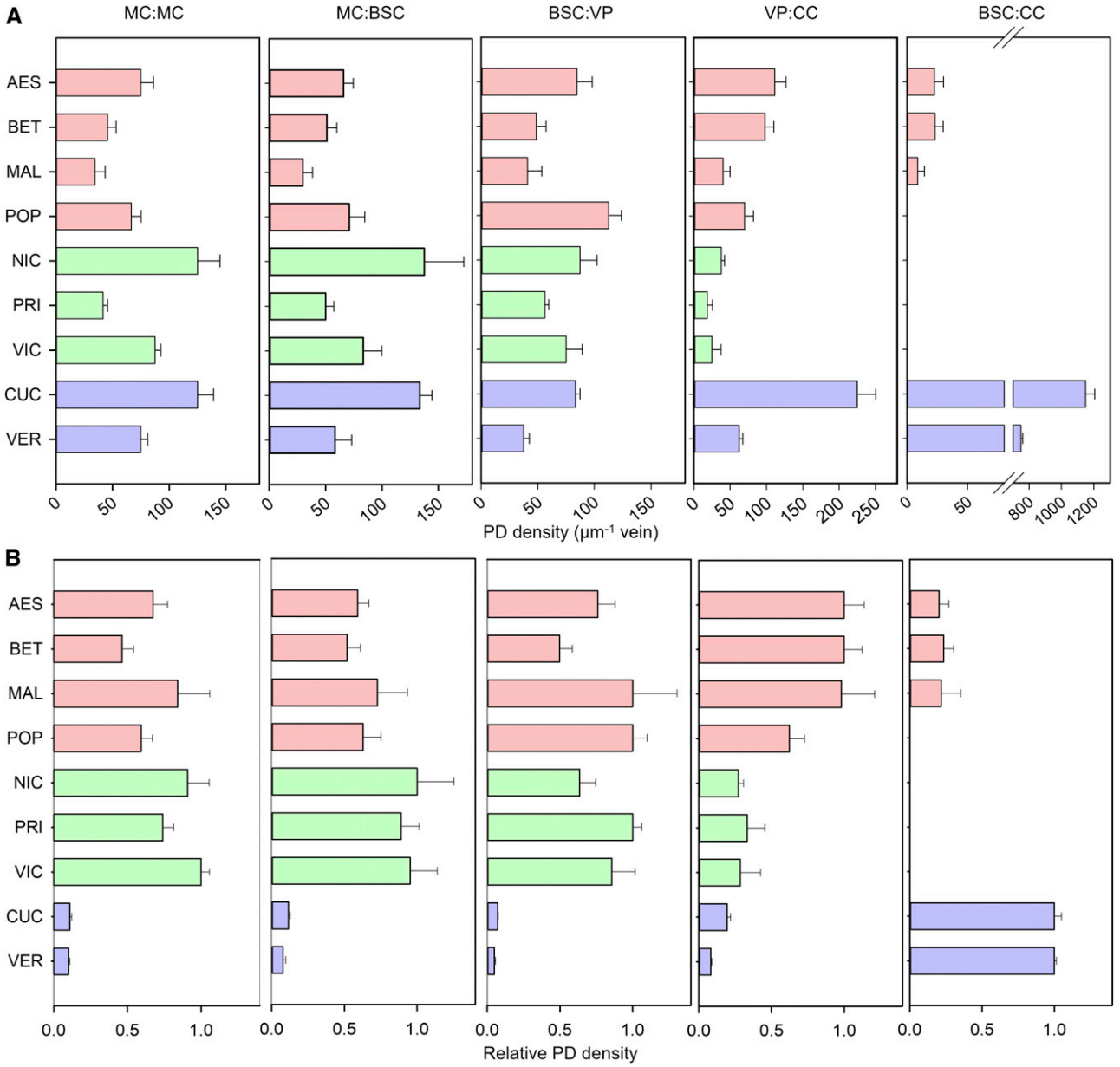

Figure 5. Plasmodesmatal density along the phloem-loading pathway. A, Density, defined as the number of PD per interface per 1 μm minor vein, in the different species. B, Relative density of PD, i.e. the PD count at each interface normalized to the highest value along the phloem-loading pathway within each species. Although absolute numbers of PD vary widely among species that have the same presumed phloem-loading type, relative density is consistent. Colors refer to the presumed phloem-loading types: passive symplasmic loading (red), active apoplasmic loading (green), and active symplasmic loading (purple). Error bars = SD. AES, *Aesculus hippocastanum*; BET, *Betula pubescens*; MAL, *Malus domestica*; POP, *Populus x canescens*; NIC, *Nicotiana tabacum*; PRI, *Primula vulgaris*; VIC, *Vicia faba*; CUC, *Cucurbita pepo*; VER, *Verbena bonariensis*.

Functional Cell Coupling Data Indicates Passive Symplasmic Loading in Trees

The data on PD function demonstrates that the four tree species tested here have a much higher functional cell coupling between phloem and bundle sheath than the active apoplasmic loaders. This corroborates the prevailing hypothesis of passive symplasmic phloem loading. In addition, relative PD density differs principally between the tree species and the five active loading species. However, the similarity of PD structure between the trees and the active apoplasmic loaders means that, potentially, relatively minor modifications of PD could lead to strong differences in permeability. Because Suc transporters are generally present in the minor veins of trees (Liesche, 2017), it could be hypothesized that a switch in loading type can happen. Because all strong gradients have been

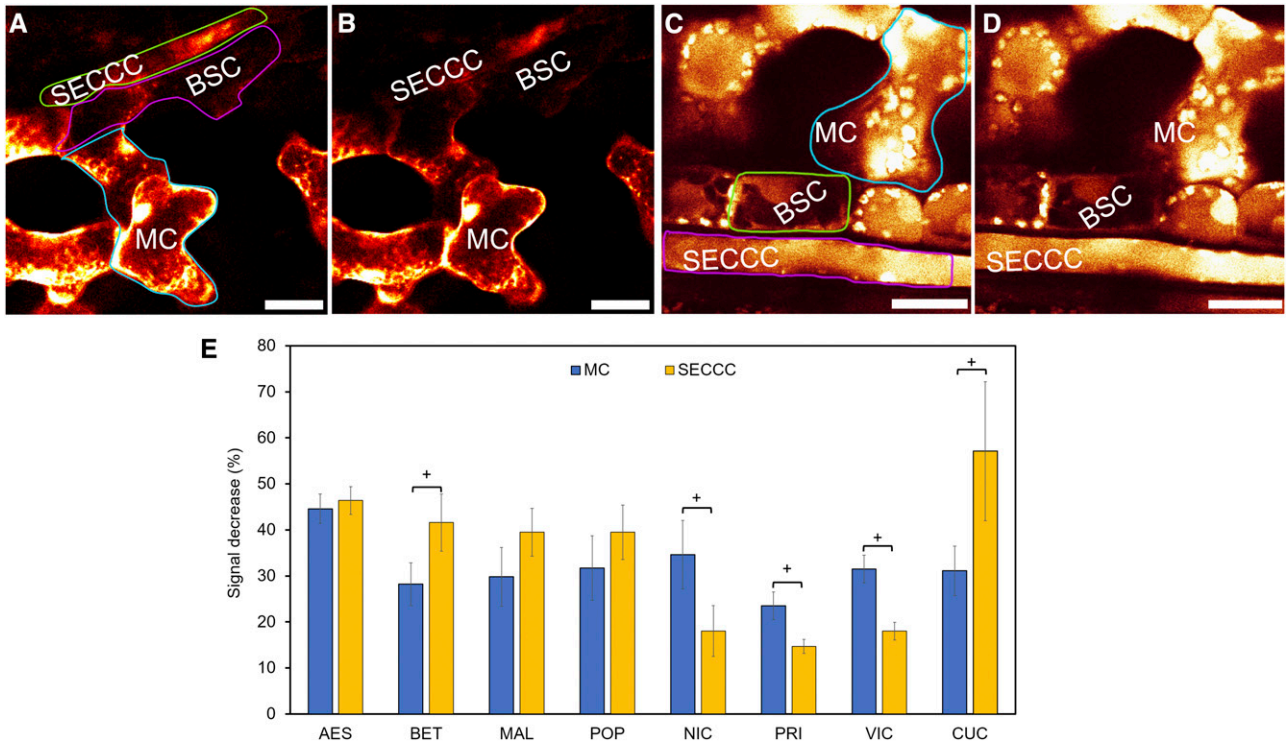

Figure 6. Quantifying plasmodesmatal function with FLIP. The fluorescence signal of the tracer CFDA was bleached in BSCs. This led to reduction of fluorescence signal in neighboring MCs and the SECCC due to tracer diffusion. A–D, Example images from *C. pepo* (A and B) and *V. faba* (C and D) show FLIP images before (A and C) and after (B and D) bleaching. Regions of interest (indicated in A and C) are used to quantify the difference in fluorescence before and after bleaching. E, Normalized reduction of fluorescence in MCs and the SECCC. Error bars = SD. Values marked by an asterisk are significantly different ($P < 0.05$). Numbers of replicates listed in Table 1. Scale bars = 20 μm. AES, *Aesculus hippocastanum*; BET, *Betula pubescens*; MAL, *Malus domestica*; POP, *Populus x canescens*; NIC, *Nicotiana tabacum*; PRI, *Primula vulgaris*; VIC, *Vicia faba*; CUC, *Cucurbita pepo*; VER, *Verbena bonariensis*.

observed in very young plants (Öner-Sieben and Lohaus, 2014; Fink et al., 2018), and the missing accumulation of sugars in mature plants (Fu et al., 2011), this could be coupled to developmental stage. However, the white birchtrees tested here were also only 2–3 years old and showed the same high functional cell coupling as the older trees.

The Phloem of Active Apoplasmic Loaders Is Not Isolated

The TEM results presented here show a surprisingly high number of PD between phloem and surrounding cells for the active apoplasmic loaders tobacco, fava bean, and primrose, considering that their phloem-loading mechanism depends on efficient transport of sugars into the phloem (Liesche and Patrick, 2017). Presence of PD at this interface has previously been reported for tobacco, but not fava bean (Gamalei, 1989). In all three species, the FLIP experiments showed a degree of coupling that is low, but significantly higher than the negative control, indicating that even in these active apoplasmic loaders, the SECCC is not completely isolated. These results match earlier observations from similar experiments using photoactivation microscopy (Liesche and Schulz, 2012). It could be speculated that the residual coupling observed here might serve the escape of signal molecules from the SECCC toward the mesophyll. PD presence at this interface must have a function, as it has negative consequences for a plant in the case of virus infestation. Viruses use these PD to enter the phloem network and, thereby, spread from one leaf to the whole plant (Harries and Ding, 2011).

Transfer Cells in *A. hippocastanum*

Another noteworthy observation is the presence of transfer cells in the minor veins of horse chestnut. Previously, presence of transfer cells has been used as a feature to classify species as active apoplasmic phloem loaders (Gamalei, 1991; Davidson et al., 2011). While transfer cells indeed occur mostly in herbaceous plants, a survey of 975 species from 242 families found them in four woody species (Pate and Gunning, 1969). Considering that horse chestnut was shown here to be a symplasmic loader, the function of transfer cells cannot be explained at present. The hypothesis that horse

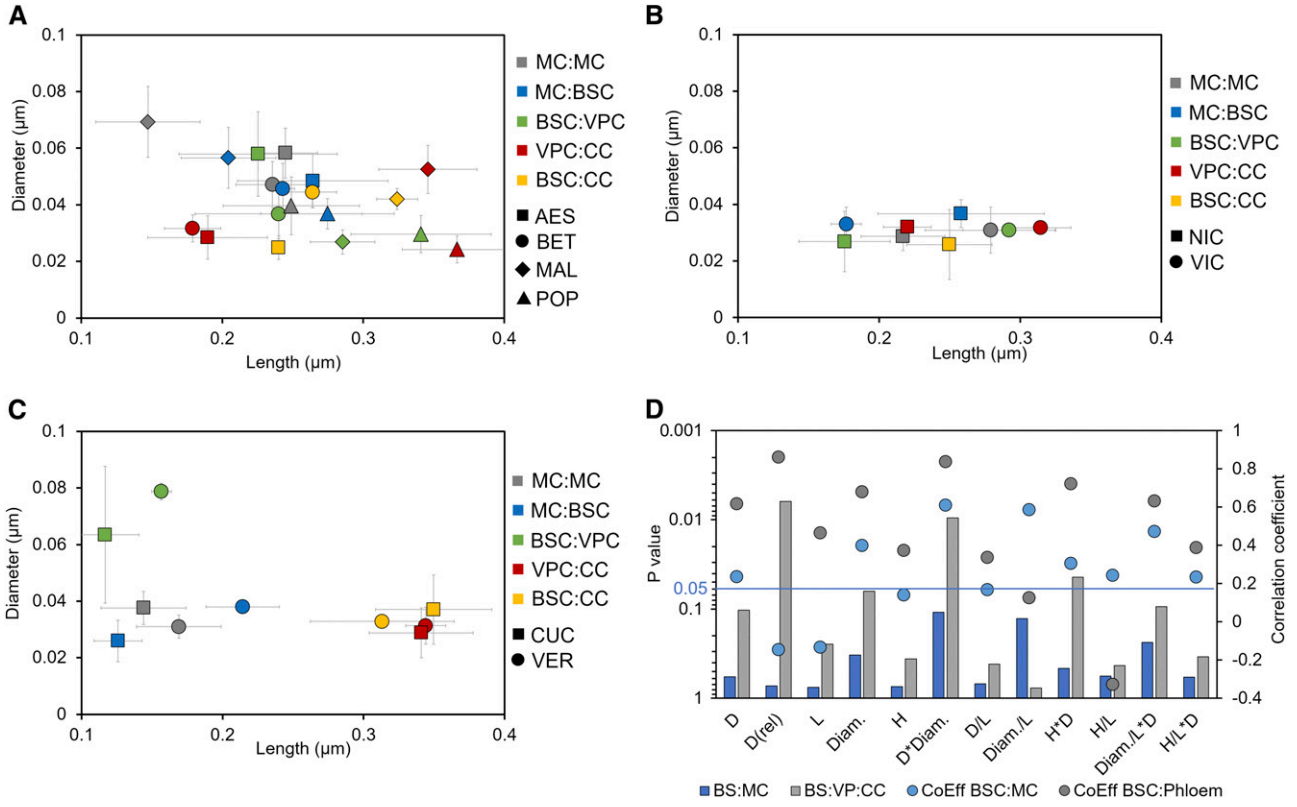

Figure 7. PD structural parameters and correlation with permeability. A–C, Relationship of PD length and diameter at different cellular interfaces. Note the large variability of PD structure between the potential passive symplasmic loaders (A), whereas there is more similarity for the active apoplasmic loaders (B) and active symplasmic loaders (C). In active symplasmic loaders (C), PD at the VPC:CC and BSC:CC interfaces differ from other interfaces, but PD with similar dimensions can be found in the other species. D, Significance of correlation of different structural parameters and their combinations with in vivo data on functional cell coupling. *P* values indicate significance, while the correlation coefficient indicates how well values fit on a line. Significant correlation ($P < 0.05$) was observed for relative PD density, the product of diameter and density and hindrance times density for the BSC:phloem interface, but not the MC:BSC interface ($n = 8$). Error bars = SD. D = Density; D(rel) = density relative to other interfaces of the phloem-loading pathway of the same species; L = PD length; Diam. = PD diameter; H = Hindrance; AES, *Aesculus hippocastanum*; BET, *Betula pubescens*; MAL, *Malus domestica*; POP, *Populus x canescens*; NIC, *Nicotiana tabacum*; PRI, *Primula vulgaris*; VIC, *Vicia faba*; CUC, *Cucurbita pepo*; VER, *Verbena bonariensis*.

chestnut is able to switch to active apoplasmic loading under certain conditions cannot be refuted, nor can a potential role in the import of specialized metabolites.

MATERIALS AND METHODS

Plant Material

All plants were grown in the Copenhagen area, Denmark (Latitude 55.67, Longitude 12.46), either in the greenhouse or outdoors (Table 1). Samples for TEM analysis were collected during June 2016. For the tree species, leaves were collected from the same individuals on at least three different days. Leaves from the middle-part of the crown, facing southward, were collected at each time point. None of the plants showed any signs of pathogen infection. For the herbaceous species, one leaf was collected from at least three different plants. In all cases, the largest or second-largest leaf was chosen. The age of specimen at the time of sampling was 6-8 years for horse chestnut (*Aesculus hippocastanum*), 2 years for white birch (*Betula pubescens*), 10 years for orchard apple (*Malus domestica*), 12 years for gray poplar (*Populus x canescens*), 8 weeks for tobacco (*Nicotiana tabacum*), 6 weeks for primrose (*Pinus vulgaris*), 6 weeks for fava bean (*Vicia faba*), 4 weeks for pumpkin (*Cucurbita pepo*), and 8 weeks for verbena (*Verbena bonariensis*). Samples for FLIP analysis were collected during July 2016 and June 2017, generally on sunny days with temperatures of between 15°C and 22°C. The sampled leaves were of similar size and at the same position as the leaves collected for TEM analysis.

Electron Microscopy

Leaf pieces of ~2×4 mm were cut out from source leaf, avoiding the larger veins. The samples were fixed for 2 h under vacuum with Karnovsky's fixative (2.5% [v/v] glutaraldehyde and 2% [w/v] formaldehyde in 0.1 M sodium cacodylate buffer, pH 7.2, all from Sigma-Aldrich). The fixative was replaced by a 0.1 M sodium cacodylate buffer, pH 7.2, and samples placed in a tissue rotator for 20 min, then washed with 0.1 M sodium cacodylate buffer and incubated another 20 min. The buffer was removed and replaced by osmium fixative (1% [w/v] osmium tetroxide in 0.1 M sodium cacodylate buffer, pH 7.2; Sigma-Aldrich). The samples were left for postfixation for 1 h in the rotator and thereafter rinsed in 0.1 M sodium cacodylate buffer and water for 20 min, respectively. Dehydration was performed by a series of 50% to 100% (v/v) acetone solutions, which were replaced every 20–30 min. Spurr's resin (Polysciences) was then added in a 1:3, 1:1, and 3:1 ratio with acetone and rotated for 30 min in each step. Pure Spurr's resin was applied and samples were left without lids for an hour so any remaining acetone could vaporize. The samples were left overnight, and the resin was changed once before embedding in flat molds in the oven at 70°C for 8 h. An EM UC7 Ultramicrotome

(Leica Microsystems) was used for making ultrathin sections of 50-nm thickness with a diamond knife. Sections were cut into a trough of water, attached to the knife. A cotton swab with chloroform was briefly held over the sections. The vapor flattens the pieces if wrinkled. A grid coated with pioloform film was held with a forceps and dipped into the water gripping three ultrathin sections. The ultrathin sections were stained with a 1% (w/v) uranyl acetate solution and a 0.5% (w/v) lead citrate solution (Reynolds, 1963). The grids were placed on a drop of uranyl acetate in a petri dish for 5 min. They were then washed by dipping into three vials with water and transferred to a new petri dish onto a drop of lead citrate for 3 min. NaOH pellets (Sigma-Aldrich) were placed in the petri dish to avoid any precipitation of lead carbonate. The grids were then washed with Milli-Q water (Millipore) and dried onto filter paper. The images were taken with a CM100 Transmission Electron Microscope (Philips) with a side-mounted 11 MP camera (Morada) set to an acceleration voltage of 80 kV and the meter at 1.72 s for each picture. Different magnifications were used ranging from 2,600X to 10,500X. The number of minor veins analyzed is given in Table 1. The number of PD were counted per minor vein and the diameter and length of each PD was measured with the software ImageJ (Schindelin et al., 2012).

Quantification of PD Structure and Calculation of Permeability

PD density was determined from electron micrographs as recommended by Robards (1976) and Botha and van Bel (1992). Any portion of a PD visible in a micrograph was counted. With a section thickness of 50 nm and an average PD diameter of 39 nm, it is unlikely that any PD was left out. To avoid double counting of PD, no directly consecutive sections were analyzed. Results were extrapolated (number of minor vein sections analyzed per species given in Table 1) to 1-μm thickness, equaling the number of PD per 1-μm minor vein length. To avoid bias and assure reliability of results, PD were counted separately by three scientists, one of them not familiar with phloem-loading types. Results were found in good agreement and average values of the counting were used.

PD diameters were measured at the neck region, which is assumed to be the part responsible for regulation of permeability (Roberts and Oparka, 2003). All PD showed the same diameter on both sides, except PD at the BSC:CC interface in active symplasmic loaders. Here the narrower CC side was measured. PD length was measured using the segmented line tool in the software ImageJ (Schindelin et al., 2012), taking the nonlinear path of PD through the wall into account.

The hindrance was calculated according to the cytoplasmic sleeve model and its analytical solution presented by Liesche and Schulz (2013). The hindrance, as calculated with this model, describes the factor by which diffusion of a solute is constrained if the solute and slit have nanometer-scale dimensions. Calculation of this parameter mainly depends on the relative size of the solute molecule to the width of the cytoplasmic sleeve. The hydrodynamic radius of Suc (4.2×10^6 $cm^2\ s^{-1}$; Liesche and Schulz, 2013), as the main sugar moving along the phloem-loading pathway, was used.

Fluorescence Microscopy

Intact herbaceous species and whole branches from the woody species were used. The mobile cytosolic tracer carboxyfluorescein (CF) was introduced into cells in ester form as 5-(and-6)-CF diacetate (CFDA, Invitrogen), Excitation/Emission = 488/517 nm. CFDA (50 μM). It was loaded into a leaf, still attached to the plant or branch. A 5×5-mm section of the abaxial epidermis region was removed with forceps to aid the dye loading into the leaf interior. Incubation time was 20 min, then the leaf was detached from the plant or branch and briefly rinsed in water before the FLIP experiment. The epidermis of birch and pumpkin were thin and difficult to remove without compromising the underlying tissue. In these cases, the abaxial leaf side was gently rubbed with sandpaper grain 600 instead.

After setting the background level, a BSC was chosen, and this target cell was repeatedly photobleached using the ZOOM-IN function in the confocal "FRAP"-Wizard module. A confocal laser scanning microscope TCS SP5X or SP8 CLSM (Leica Microsystems) was used for visualization of the fluorescent probe. The Argon laser power was 25% power. The emission band pass for detection was set to 507 nm to 537 nm. A 20× water immersion objective was used in all FLIP experiments. Line average was set to 1 and laser line 488 nm was set to 100% during bleaching, and 20% for both pre- and postbleach. Time settings were five frames before/after and 50 frames during bleaching, with acquisition of one frame taking 1.2 s. Any cell that is connected to the target cell by PD will gradually lose fluorescence as the bleached dye molecules diffuse into this area. By contrast, the fluorescence in unconnected regions will not be affected. A preimage and a postimage were used for calculation of the percentage intensity decrease for the target BSC and directly neighboring MC and phloem cells. The decrease was normalized in relation to the target BSC fluorescence to compensate for differences in the bleaching efficiency between experiments. This is necessary, because diffusion of CF depends on tracer concentration potential, in addition to interface permeability. Differences in cell size were not considered, because most of the tracer moves within the first seconds of the experiment, when the concentration potential between BSC and MC and between BSC and SECCC is the same. The initial CF concentration is the same in all cells. Moreover, the cell size-ratio of MC and SECCC is similar in all species, ~1.5:1. This means that the slight error that is introduced is similar in all species and does not impact the assessment of relative symplasmic coupling. Diffusion of CF is similar to diffusion of Suc, because their hydrodynamic radius is almost identical (Liesche and Schulz, 2013). Number of experiments per species are listed in Table 1.

Statistics

The significance of correlations was tested using Pearson Product Moment correlation as implemented in SigmaPlot (Version 12.5; Systat Software). A correlation was considered significant when the P value was <0.05. The significance of two data points being significantly different was tested using Welch's t test as implemented in Excel (Microsoft). A difference with P value <0.05 was considered significant.

Supplemental Data

The following supplemental material is available:

Supplemental Figure S1. FLIP control experiments.

ACKNOWLEDGMENTS

We thank Eva Deinum, University of Wageningen for critical reading of the manuscript. Imaging was performed at the Center for Advanced Bioimaging Denmark and at the Northwest A&F University Life Science Research Core Services.

Received November 1, 2018; accepted January 28, 2019; published February 5, 2019.

LITERATURE CITED

Adams III WW, Cohu CM, Amiard V, Demmig-Adams B (2014) Associations between the acclimation of phloem-cell wall ingrowths in minor veins and maximal photosynthesis rate. Front Plant Sci **5:** 24

Batashev DR, Pakhomova MV, Razumovskaya AV, Voitsekhovskaja OV, Gamalei YV (2013) Cytology of the minor-vein phloem in 320 species from the subclass Asteridae suggests a high diversity of phloem-loading modes. Front Plant Sci **4:** 312

Botha CEJ, van Bel AJE (1992) Quantification of symplastic continuity as visualised by plasmodesmograms: diagnostic value for phloem-loading pathways. Planta **187:** 359–366

Braun DM (2012) Plant science. SWEET! The pathway is complete. Science **335:** 173–174

Davidson A, Keller F, Turgeon R (2011) Phloem loading, plant growth form, and climate. Protoplasma **248:** 153–163

Ding B, Turgeon R, Parthasarathy MV (1992) Substructure of freeze-substituted plasmodesmata. Protoplasma **169:** 28–41

Fink D, Dobbelstein E, Barbian A, Lohaus G (2018) Ratio of sugar concentrations in the phloem sap and the cytosol of mesophyll cells in different tree species as an indicator of the phloem loading mechanism. Planta **248:** 661–673

Fu Q, Cheng L, Guo Y, Turgeon R (2011) Phloem loading strategies and water relations in trees and herbaceous plants. Plant Physiol **157:** 1518–1527

Gamalei Y (1989) Structure and function of leaf minor veins in trees and herbs. Trees (Berl) **3:** 96–110

Gamalei Y (1991) Phloem loading and its development related to plant evolution from trees to herbs. Trees (Berl) **5:** 50–64

Goggin FL, Medville R, Turgeon R (2001) Phloem loading in the tulip tree. Mechanisms and evolutionary implications. Plant Physiol **125:** 891–899

Harries P, Ding B (2011) Cellular factors in plant virus movement: At the leading edge of macromolecular trafficking in plants. Virology **411:** 237–243

Knox K, Wang P, Kriechbaumer V, Tilsner J, Frigerio L, Sparkes I, Hawes C, Oparka K (2015) Putting the squeeze on plasmodesmata: A role for reticulons in primary plasmodesmata formation. Plant Physiol **168:** 1563–1572

Liesche J (2017) Sucrose transporters and plasmodesmal regulation in passive phloem loading. J Integr Plant Biol **59:** 311–321

Liesche J, Patrick J (2017) An update on phloem transport: A simple bulk flow under complex regulation. F1000 Res **6:** 2096

Liesche J, Schulz A (2012) *In vivo* quantification of cell coupling in plants with different phloem-loading strategies. Plant Physiol **159:** 355–365

Liesche J, Schulz A (2013) Modeling the parameters for plasmodesmal sugar filtering in active symplasmic phloem loaders. Front Plant Sci **4:** 207

Martens HJ, Roberts AG, Oparka KJ, Schulz A (2006) Quantification of plasmodesmatal endoplasmic reticulum coupling between sieve elements and companion cells using fluorescence redistribution after photobleaching. Plant Physiol **142:** 471–480

Nicolas WJ, Grison MS, Trépout S, Gaston A, Fouché M, Cordelières FP, Oparka K, Tilsner J, Brocard L, Bayer EM (2017) Architecture and permeability of post-cytokinesis plasmodesmata lacking cytoplasmic sleeves. Nat Plants **3:** 17082

Öner-Sieben S, Lohaus G (2014) Apoplastic and symplastic phloem loading in *Quercus robur* and *Fraxinus excelsior*. J Exp Bot **65:** 1905–1916

Oparka K, Prior DAM (1992) Direct evidence for pressure-generated closure of plasmodesmata. Plant J **2:** 741–750

Pate JS, Gunning BES (1969) Vascular transfer cells in angiosperm leaves, a taxonomic and morphological survey. Protoplasma **68:** 135–156

Rennie EA, Turgeon R (2009) A comprehensive picture of phloem loading strategies. Proc Natl Acad Sci USA **106:** 14162–14167

Reynolds ES (1963) The use of lead citrate at high pH as an electron-opaque stain in electron microscopy. J Cell Biol **17:** 208–212

Robards AW (1976) Plasmodesmata in higher plants. *In* BES Gunning and AW Robards, eds, Intercellular Communication in Plants: Studies on Plasmodesmata. Springer, Berlin, Heidelberg

Roberts AG, Oparka K (2003) Plasmodesmata and the control of symplastic transport. Plant Cell Environ **26:** 103–124

Schindelin J, Arganda-Carreras I, Frise E, Kaynig V, Longair M, Pietzsch T, Preibisch S, Rueden C, Saalfeld S, Schmid B, et al (2012) FIJI: An open-source platform for biological-image analysis. Nat Methods **9:** 676–682

Schulz A (1995) Plasmodesmal widening accompanies the short-term increase in symplasmic phloem unloading in pea root tips under osmotic stress. Protoplasma **188:** 22–37

Schulz A (1999) Physiological control of plasmodesmal gating. *In* AJE van Bel and WJP van Kesteren, eds, Plasmodesmata. Springer, Berlin, Heidelberg, New York, pp 173–204

Schulz A (2015) Diffusion or bulk flow: How plasmodesmata facilitate prephloem transport of assimilates. J Plant Res **128:** 49–61

Turgeon R, Medville R (2004) Phloem loading. A reevaluation of the relationship between plasmodesmatal frequencies and loading strategies. Plant Physiol **136:** 3795–3803

Zhang C, Turgeon R (2018) Mechanisms of phloem loading. Curr Opin Plant Biol **43:** 71–75